

A SIMPLE APPROACH TO FABRICATE g-C₃N₄/MoS₂ NANOCOMPOSITE AND ITS APPLICATION AS A LUBRICANT ADDITIVE

Z. D. XU^a, J. B. XIN^a, R. X. FAN^a, K. WANG^b, J. YANG^{c,*}

^a State Grid Jiangxi Electric Power Company, Electric Power Research Institute, Nanchang, 330096, P.R. China

^b State Grid Jiangxi Electric Power Company, Nanchang, 330096, P.R. China

^c Institute for Advanced Materials, School of Materials Science and Engineering, Jiangsu University, Zhenjiang, 212013, P.R. China

The graphitic carbon nitride/molybdenum disulfide (g-C₃N₄/MoS₂) nanocomposite was synthesized by a simple hydrothermal process. MoS₂ and g-C₃N₄ were coexisted by the chemical bonding with high purity and the layered MoS₂ well dispersed on g-C₃N₄ nanosheets. The tribological property of g-C₃N₄/MoS₂ nanocomposite was systematically investigated under different conditions used as the lubricant additive, and the results indicated that the introduction of g-C₃N₄/MoS₂ nanocomposite into base oil could reduce friction and wear drastically, which was better than the testing results of single MoS₂, g-C₃N₄ and the mixture of MoS₂ and g-C₃N₄. The excellent tribological property of the MoS₂/g-C₃N₄ nanocomposite can be explained by the excellent traction and support effects of g-C₃N₄, and the synergistic friction reduction and wear-resistant effects of g-C₃N₄ and MoS₂ nanosheets. This work highlights a pathway to expand potential applications of MoS₂ and g-C₃N₄ based materials in the tribology field.

(Received April 18, 2018; Accepted August 13, 2018)

Keywords: g-C₃N₄; MoS₂, Nanocomposite, Tribology

1. Introduction

Recently, high efficient and stable tribology materials have attracted extensive attention with the rapid development of machinery industry [1]. Carbon-based nanomaterials such as graphite, fullerene, carbon nanotubes, and graphene, have been widely studied in the fields of tribology [2-5]. These materials, especially graphene, could form conformal protective coatings on sliding contact interfaces, thus drastically reducing the wear. Subsequently, ultrathin two-dimensional (2D) materials promoted tribology into an interesting research area [6]. Graphitic carbon nitride (g-C₃N₄) as a class of polymeric materials consisting mainly of carbon and nitrogen possesses a two-dimensional (2D) structure stacked by weak Van der Waals interactions, which facilitates the exfoliation of bulk crystals for the production of 2D g-C₃N₄ [7]. Meanwhile, this 2D structure can result in a low shear resistance and provide the excellent tribological properties. Zhu et al. fabricated the g-C₃N₄/poly(vinylidene difluoride) (PVDF) composites and found that the

*Corresponding author: yangjin@ujs.edu.cn

g-C₃N₄ filler was beneficial to reduce wear loss of the composite [8]. In our previous work, we also found that g-C₃N₄ nanosheets can greatly enhance the friction-reducing and anti-friction properties of base oil [9]. However, it is difficult for a single 2D nanomaterial to meet the requirements of tribological properties.

Molybdenum disulfide (MoS₂), as a typical lubricant, has been widely used for the industry lubrication due to the crystallographic structure consisting of the covalently bonded S-Mo-S tri-layers and easy sliding between layers under the shearing force [10-12]. The Young's modulus of monolayer MoS₂ nanosheet is 270 ± 100 GPa which is superior to that of steel (210 GPa) and the corresponding in-plane stiffness is 180 ± 60 N/m. The strong intralayer covalent bonding and weak interlayer interaction endow 2D MoS₂ with promising lubrication prospect. Li et al. demonstrated a method to study the frictional properties between atomic layers of MoS₂ and found that the friction coefficient of a monolayer MoS₂ nanosheet on incommensurate MoS₂ substrate was about 10^{-4} (belong to the area of superlubricity) [13]. Moreover, Hou and Leven et al. demonstrated that heterostructures constructed by stacking two kinds of 2D nanomaterials, such as graphene/MoS₂ and graphene/h-BN, show nearly two orders of magnitude reduction of interlayer shear strength compared with homogeneous bilayers [14-15]. Based on the above works, coupling 2D g-C₃N₄ nanosheets with MoS₂ nanosheets is probably one of the most ideal choices for constructing heterostructures with high efficient and stable tribological properties, but the relevant report is seldom.

In this paper, the g-C₃N₄/MoS₂ nanocomposite was synthesized through a one-step hydrothermal method and its tribological property was investigated as a lubricant additive. Base oil was chosen because of its poor lubricating property, which can more clearly reflect the improvement effect of the g-C₃N₄/MoS₂ nanocomposite. The results confirmed that the obtained g-C₃N₄/MoS₂ can obviously reduce the friction coefficient and enhance the anti-wear ability compared to single MoS₂, g-C₃N₄ and the mixture of MoS₂ and g-C₃N₄. The details of synthesis, characterization, and tribological property of the g-C₃N₄/MoS₂ nanocomposite were described herein.

2. Experimental

2.1. Synthesis of the g-C₃N₄/MoS₂ nanocomposite

g-C₃N₄ was firstly prepared by a solid reaction process using urea [16]. Subsequently, g-C₃N₄ (0.20g) was added into a beaker with distilled water (20 mL) under ultrasonic treatment for 2 h. (NH₄)₆Mo₇O₂₄•4H₂O (0.50g), HONH₃Cl (1.0g), and C₁₆H₃₃(CH₃)₃NBr (0.1g) were dissolved in distilled water (20 mL), and added into the g-C₃N₄ dispersion with magnetic stirring for 0.5 h. Then, CH₂H₄S (0.45g) was dissolved in distilled water (10 mL) and added into the above solution. Finally, the solution was transferred into a Teflon-lined autoclave (100 mL) and placed in an electric oven with 200 °C for 24 h. The as-prepared g-C₃N₄/MoS₂ nanocomposites were washed with distilled water and ethanol for several times and then dried in a vacuum oven at 60 °C for 10 h. For comparison, MoS₂ were synthesized following the same procedure without the addition of g-C₃N₄.

2.2 Friction and wear tests

Tribological properties of the base oils containing samples (5 wt%) were studied with an UMT-2 tribometer (CETR Corporation Ltd, USA) in a ball-on-disk configuration. The variation of friction coefficient under different loads and speeds was investigated. The testing was performed under a normal load of 6-30 N, at a rotating speed of 100-400 rpm, a relative humidity of 50-60%, and duration of 10 min. The stainless steel ball with a diameter of 3 mm and a hardness of 62 HRC was made of 9Cr18 steel, and the counterpart was 45# steel disk of \varnothing 20 mm \times 3 mm in size. The wear scar was measured by the VEECO WYKO NT1100 non-contact optical profile testing instrument.

2.3. Characterization

X-ray diffraction (XRD) analysis was carried out using diffractometer (D8 Advance, Bruker, Germany) with Cu K α radiation ($\lambda = 0.1546$ nm) in the range of 5-80°. Raman spectra (Advantage 633, DeltaNu, USA) were performed with an excitation laser of 532 nm in wavelength. X-ray photoelectron spectroscopy (XPS) analysis was measured using an X-ray photoelectron spectrometer (Escalab 250Xi, ULVCA-PHI, USA) with Al K α radiation. Scanning electron microscopy (SEM) measurements were carried out using field emission scanning electron microscopy (JSM-7001F, JEOL, Japan). Transmission electron microscope (TEM) measurements were carried out using high-resolution microscope (JEOL-2010, JEOL, Japan) instrument, operating at an accelerating voltage of 200 kV.

3. Results and discussion

3.1. Structural and morphological analysis

XRD patterns of the as-prepared g-C₃N₄, MoS₂ and g-C₃N₄/MoS₂ are shown in Fig. 1a. For g-C₃N₄/MoS₂, there are three obvious peaks at 14.1°, 34°, and 57° corresponding to the (002), (100) and (110) planes of MoS₂.

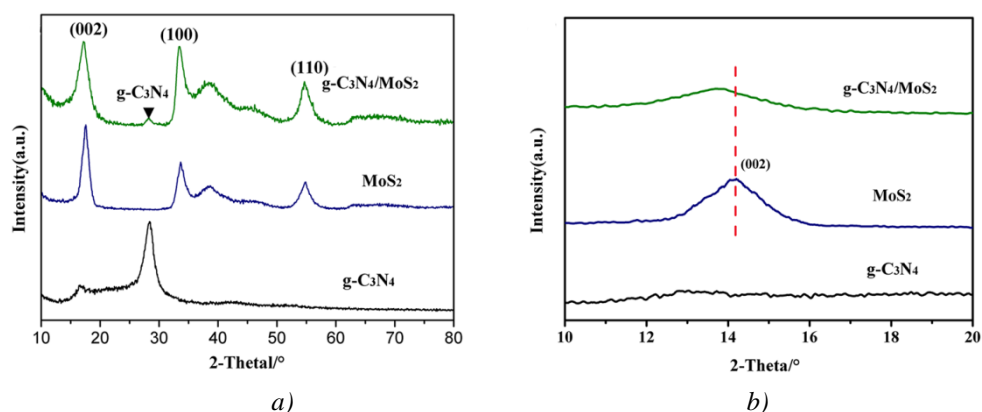


Fig. 1. (a) XRD patterns of g-C₃N₄, MoS₂, and g-C₃N₄/MoS₂. (b) The enlarged of 002 peak for g-C₃N₄, MoS₂, and g-C₃N₄/MoS₂

In addition, the peak at 27.4° corresponds to the (002) plane of $g\text{-C}_3\text{N}_4$ [17]. As shown in Fig.1b The major XRD peak at 14.2° corresponds to the (002) reflections of closely stacked layered structure with an interlayer spacing of 6.20 \AA [18]. But this peak for $g\text{-C}_3\text{N}_4/\text{MoS}_2$ was shift towards low-angle region, which indicates that the interlamellar spacing of MoS_2 was broadened when combined with $g\text{-C}_3\text{N}_4$ [19]. No other peaks for impurities were detected. These results proved that MoS_2 is well combined with $g\text{-C}_3\text{N}_4$ with high chemical purity.

Raman spectra of MoS_2 , $g\text{-C}_3\text{N}_4$ and $g\text{-C}_3\text{N}_4/\text{MoS}_2$ are shown in Fig. 2. The two dominant peaks of MoS_2 and $g\text{-C}_3\text{N}_4/\text{MoS}_2$ at 377 and 403 cm^{-1} correspond to E_{2g}^1 and A_{1g} modes of the hexagonal MoS_2 , respectively. The E_{2g}^1 mode involves the in-layer displacement of Mo and S atoms, whereas the A_{1g} mode involves the out-of-layer symmetric displacement of S atoms along the c axis [20].

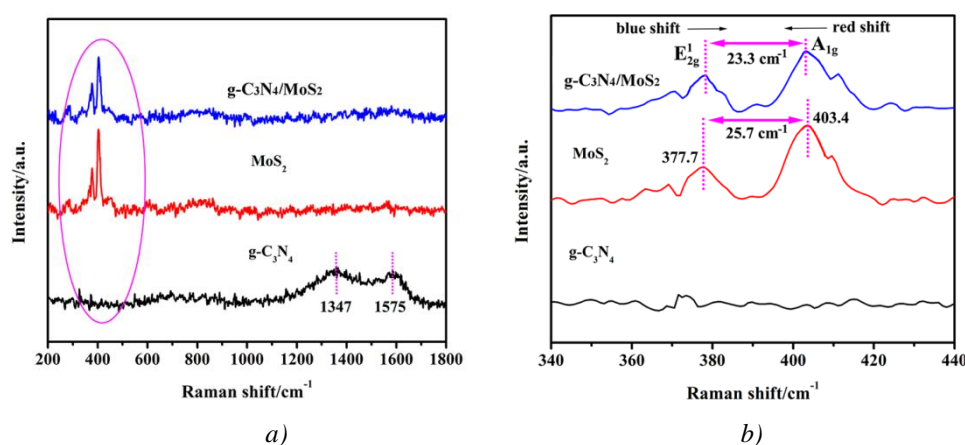


Fig. 2. (a) Raman spectra of $g\text{-C}_3\text{N}_4$, MoS_2 , and $g\text{-C}_3\text{N}_4/\text{MoS}_2$.
(b) The enlarged peak at 400 cm^{-1} for $g\text{-C}_3\text{N}_4$, MoS_2 , and $g\text{-C}_3\text{N}_4/\text{MoS}_2$

It can be found in Fig. 2b that the peak position interval of MoS_2 in $\text{MoS}_2/g\text{-C}_3\text{N}_4$ is diminished by compared to the peak position interval of single MoS_2 . In addition, two other Raman peaks at 1347 and 1575 cm^{-1} can be detected in the spectra of $g\text{-C}_3\text{N}_4$ and $g\text{-C}_3\text{N}_4/\text{MoS}_2$, which are related to the D and G bands of graphite-like D and G peaks, confirming the graphitic layered structure of the prepared $g\text{-C}_3\text{N}_4$. These results suggest that the $g\text{-C}_3\text{N}_4/\text{MoS}_2$ nanocomposites were successfully synthesized.

In order to verify the components and chemical status of the as-prepared products, XPS measurement was conducted on the obtained $g\text{-C}_3\text{N}_4/\text{MoS}_2$ nanocomposites. As shown in Fig. 3, the sample contained elements of Mo, S, C, and N, and the survey XPS spectrum of $g\text{-C}_3\text{N}_4/\text{MoS}_2$ reveals peaks for C, N, Mo, and S (Fig.3a). The high resolution XPS spectrum of $\text{Mo}3d$ shows two peaks at 229.8 and 232.9 eV corresponding to $\text{Mo}3d^{3/2}$ and $\text{Mo}3d^{5/2}$ of Mo^{4+} (Fig. 3b), respectively, whereas the peaks at 162.6 and 163.8 eV in $\text{S}2p$ spectra are associated with $\text{S} 2p^{1/2}$ and $\text{S}2p^{3/2}$ of S^{2-} (Fig.3c), respectively. These XPS results are in good agreements with previous reports of exfoliated MoS_2 [21]. As shown in Fig. 3d, three peaks centering at 284.7 , 286.6 , and 288.85 eV can be found in the high resolution XPS spectrum of $\text{C}1s$. The peak at 284.7 eV was assigned the adventitious carbon on the surface of $g\text{-C}_3\text{N}_4$. The $\text{N}1s$ high-resolution spectrum in Fig. 3e could be fitted into three peaks. The peak at 397.9 eV was typically attributed to N atoms sp^2 -bonded to two

carbon atoms (C=N-C), thus confirming the presence of sp^2 -bonded g- C_3N_4 . Two peaks at 399.85 and 401.68 eV could be assigned to tertiary nitrogen ($N-(C)_3$) and amino functional groups having a hydrogen atom (C-N-H) [22]. Therefore, it can be concluded that MoS_2 decorated g- C_3N_4 nanocomposites were successfully synthesized.

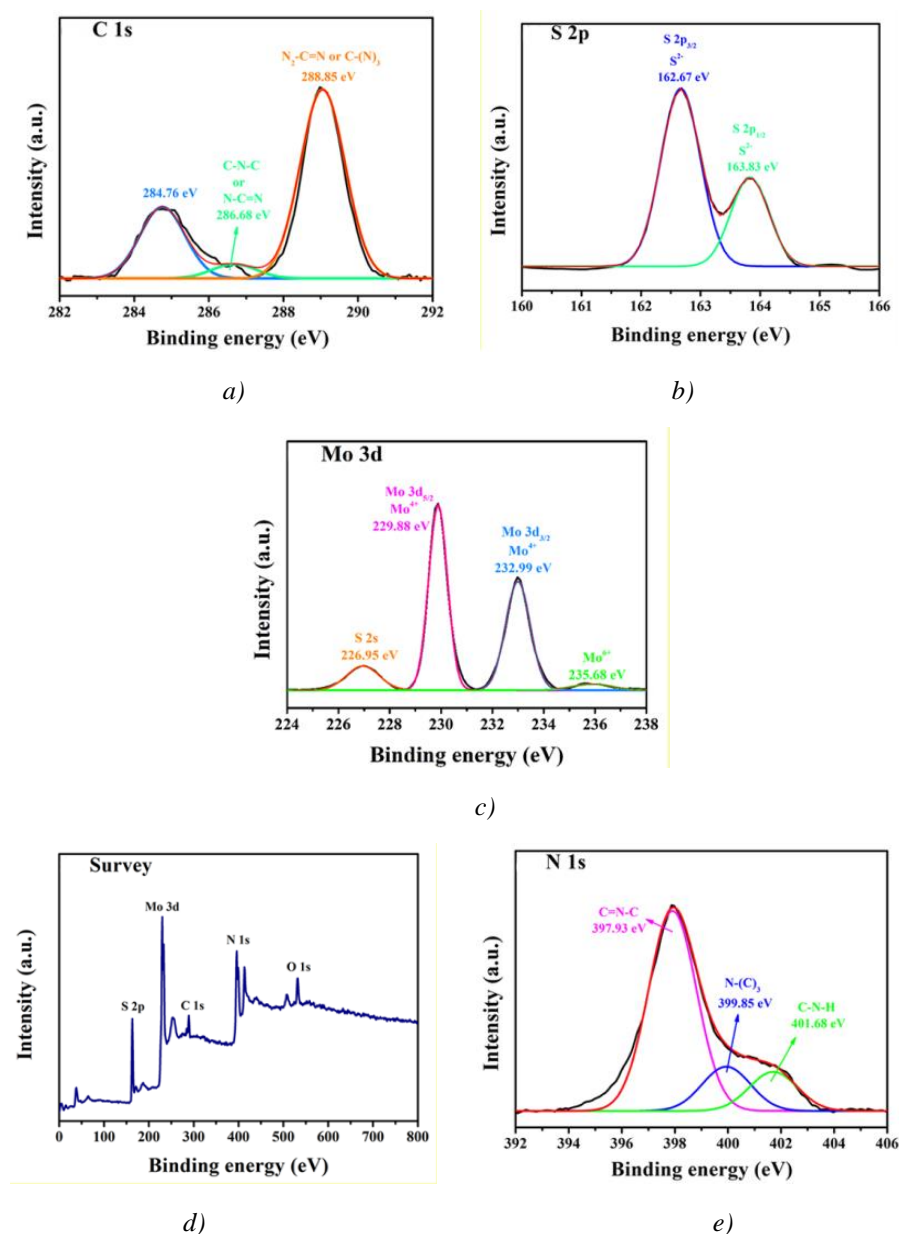


Fig. 3. (a) XPS survey spectrum of g- C_3N_4/MoS_2 . (b), (c), (d) and (e) Narrow scan spectra of Mo3d, S2p, C1s, and N1s of g- C_3N_4/MoS_2

The morphology characterizations of g- C_3N_4 , MoS_2 , and g- C_3N_4/MoS_2 are shown in Fig. 4, respectively. As shown in Fig. 4a, the as-prepared g- C_3N_4 presents a typical sheet structure and the surfaces are very smooth. It can be seen in Fig. 4b that MoS_2 with the flower-like microstructure is obtained. As shown in Fig. 4c, the smooth surfaces of g- C_3N_4 nanosheets become rough with a large number of MoS_2 nanoparticles. The enlarged SEM image (Fig. 4d) further shows that MoS_2

nanoparticles exhibit the typical layer structures combined with g-C₃N₄ nanosheets uniformly, which indicates the formation of 2D g-C₃N₄/MoS₂ heterostructures.

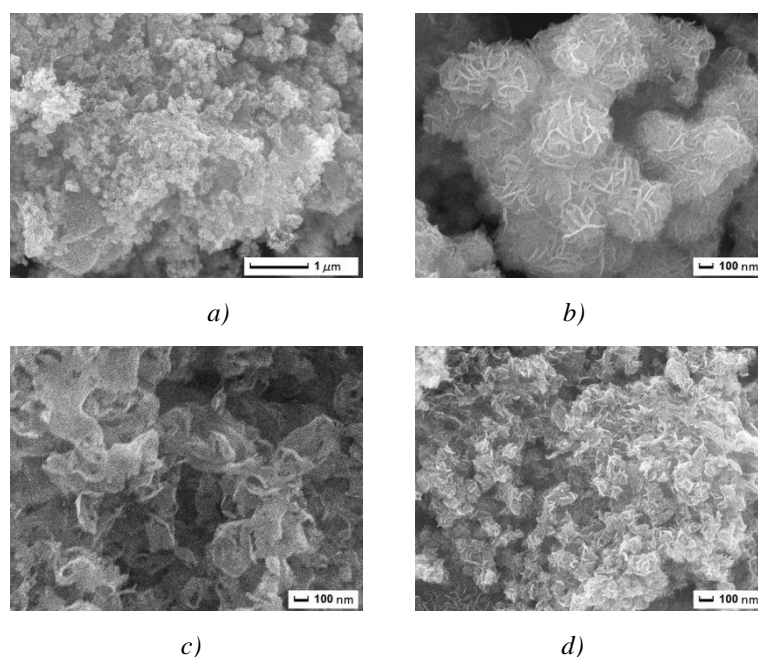


Fig. 4. SEM images of (a) g-C₃N₄, (b) MoS₂, and (c) g-C₃N₄/MoS₂. (d) The enlarged SEM image of g-C₃N₄/MoS₂

To further investigate the microstructures of g-C₃N₄/MoS₂ nanocomposites, TEM observation was performed and shown in Fig. 5. As shown in Fig. 5(a,b), the g-C₃N₄ sheets are quite thin and exhibit individual layer or stack of several layers. The pure MoS₂ show the flower-like structure assembled by nanosheets. For the g-C₃N₄/MoS₂ nanocomposites, it can be seen from Fig. 5(d,e) that MoS₂ nanosheets are homogeneously and closely distributed on the surface of g-C₃N₄ nanosheets which is corresponding to the results of SEM. High resolution TEM image (Fig. 5f) shows that the interlayer spacing of 0.63 nm measured from lattice fringes ascribed to the (002) direction of cubic structured MoS₂, which is corresponding to the result of XRD.

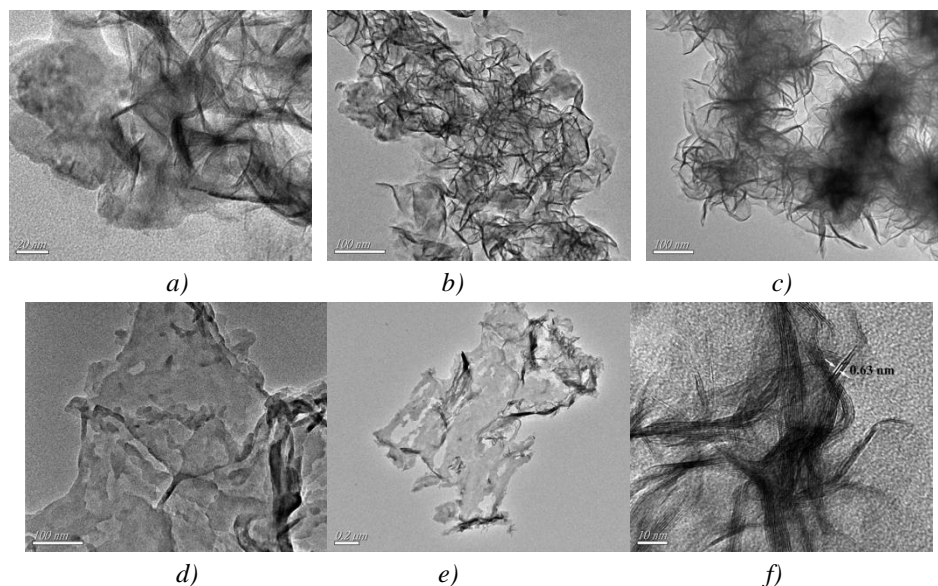


Fig. 5. TEM images of (a-b) $g-C_3N_4$, (c) MoS_2 , and (d) $g-C_3N_4/MoS_2$. (e-f) The enlarged TEM image of $g-C_3N_4/MoS_2$

3.2. Effect of $MoS_2/g-C_3N_4$ on tribological properties

Tribological properties of paraffin oil, $g-C_3N_4$, MoS_2 , the mixture of $g-C_3N_4$ and MoS_2 , and $g-C_3N_4/MoS_2$ were tested under a load of 10 N for 10 min. As shown in Fig. 6, the friction coefficient of paraffin oil was very high.

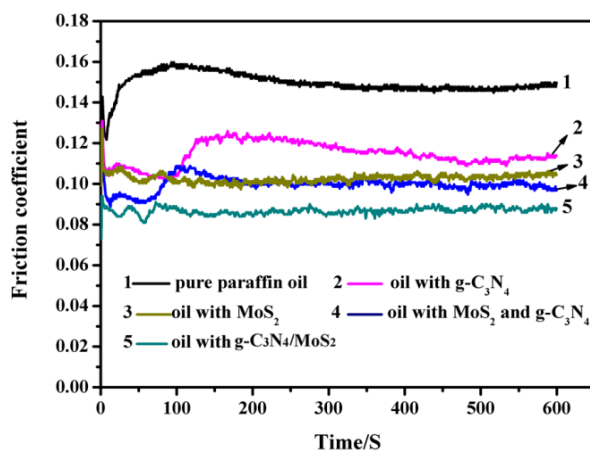


Fig. 6. Friction coefficients of paraffin oil, $g-C_3N_4$, MoS_2 , the mixture of $g-C_3N_4$ and MoS_2 , and $g-C_3N_4/MoS_2$.

When $g-C_3N_4$, MoS_2 , the mixture of $g-C_3N_4$ and MoS_2 , and $g-C_3N_4/MoS_2$ were added into paraffin oil, the coefficients of friction showed an obvious reduction. Particularly, $g-C_3N_4/MoS_2$ exhibited the best lubricating behavior with the lowest friction coefficient, and it also confirmed that the lubricating ability of $g-C_3N_4/MoS_2$ was better than that of the mixture of $g-C_3N_4$ and MoS_2 .

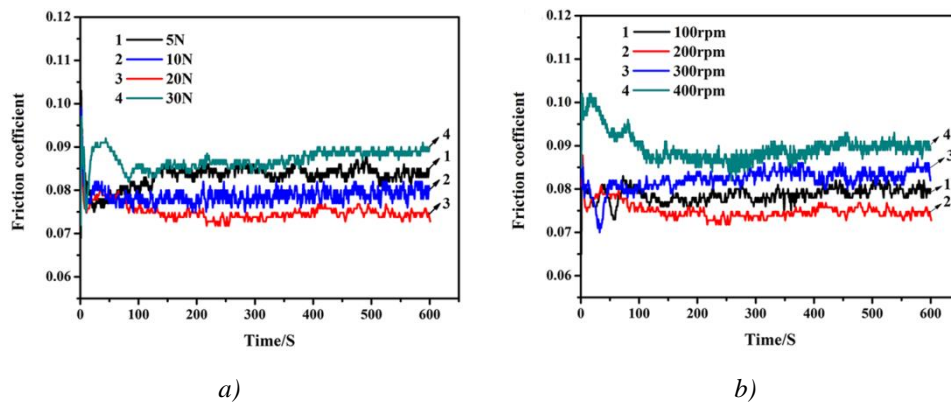


Fig. 7. The coefficients of friction of $g\text{-C}_3\text{N}_4/\text{MoS}_2$ under different (a) applied loads and (b) friction speed

To further investigate the tribological performances of $g\text{-C}_3\text{N}_4/\text{MoS}_2$ in paraffin oil, friction tests were conducted under different loads (5, 10, 20, and 30 N) and different speed (100, 200, 300, and 400 rpm). As shown in Fig. 7a, the lowest friction coefficient is corresponding to the applied load of 20N, which is represented the optimal value. It was shown in Fig. 7b that the lowest coefficients of friction is corresponding to the applied friction speed of 200 rpm. These results confirmed that $g\text{-C}_3\text{N}_4/\text{MoS}_2$ has the best friction-reducing property under the applied load of 20 N and friction speed of 200 rpm.

Fig. 8 shows the SEM and three-dimensional and morphologies of wear surfaces lubricated by paraffin oil, MoS₂, and $g\text{-C}_3\text{N}_4/\text{MoS}_2$. As can be seen from images (Fig. 8a-c), wear scar lubricated with paraffin oil is very wide and deep, indicating serious wear occurred. The addition of MoS₂ can make the worn surface become relatively narrow and shallow (Fig. 8d-f), suggesting that MoS₂ have a certain extent wear-resistant property in this case. In marked contrast, when $g\text{-C}_3\text{N}_4/\text{MoS}_2$ was added into paraffin oil, the width of wear scar remarkably becomes narrow and the friction scuffing also become more shallow and smoother (Fig. 8g-i), which proves that $g\text{-C}_3\text{N}_4/\text{MoS}_2$ nanocomposites as additive in paraffin oil can dramatically reduce the wear of steel/steel contact. This is consistent with the result of wear volume, which is diminished gradually.

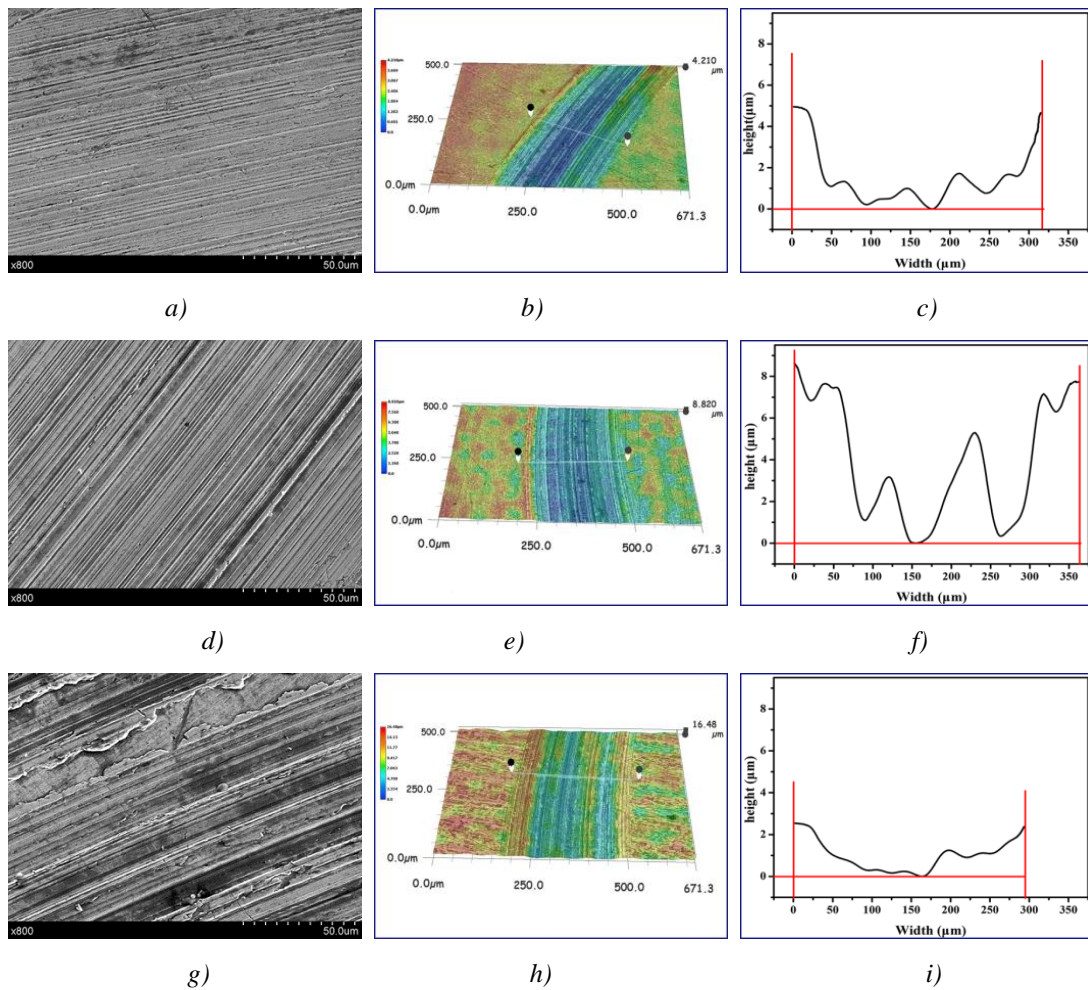


Fig. 8. SEM images and noncontact three-dimensional cross-section images of worn surfaces for (a-c) paraffin oil, (d-f) MoS_2 , and (g-i) $\text{g-C}_3\text{N}_4/\text{MoS}_2$

In order to explore the tribological mechanism of $\text{g-C}_3\text{N}_4/\text{MoS}_2$, the tribology models of $\text{g-C}_3\text{N}_4/\text{MoS}_2$ in base oil is proposed and depicted in Fig. 9. The $\text{g-C}_3\text{N}_4/\text{MoS}_2$ nanocomposite inherits both the preminent lubricating properties of MoS_2 and the outstanding wear-resistant performances of $\text{g-C}_3\text{N}_4$ nanosheets. The $\text{g-C}_3\text{N}_4$ nanosheets not only resist wear but also act as spacers to prevent the MoS_2 nanosheets from restacking. The $\text{g-C}_3\text{N}_4$ nanosheets in turn offers a perfect carrier to load the MoS_2 nanosheets, making the nanosheets work better in the oil without agglomeration. Moreover, due to the lamellar structure and the excellent dispersibility, $\text{g-C}_3\text{N}_4/\text{MoS}_2$ can easily move into the interface of the friction pair with oil and form a lubricating film during the sliding, preventing the direct contact between asperities. At the same time, the existence of MoS_2 nanosheets further increases the microhardness of $\text{g-C}_3\text{N}_4$, which makes the $\text{g-C}_3\text{N}_4/\text{MoS}_2$ more enduring [23]. Therefore, the lubricating oil film containing $\text{g-C}_3\text{N}_4/\text{MoS}_2$ can bear higher shear forces and cannot be torn easily, resulting in the reduction of friction and wear.

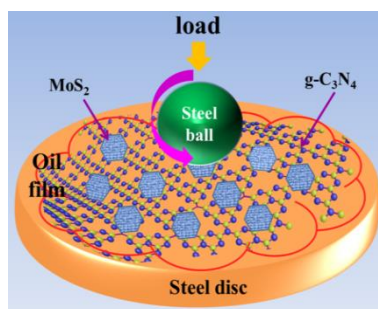


Fig. 9. Schematic illustration of tribological mechanisms of $g\text{-C}_3\text{N}_4/\text{MoS}_2$

4. Conclusions

The $g\text{-C}_3\text{N}_4/\text{MoS}_2$ nanocomposite possessing excellent tribological property was prepared by a simple hydrothermal method. Physical characterizations confirmed that the well-controlled morphology of MoS_2 nanosheets and the structural features of the $g\text{-C}_3\text{N}_4/\text{MoS}_2$ nanocomposite. Due to the unique supporting effect of $g\text{-C}_3\text{N}_4$ nanosheets, the as-prepared $g\text{-C}_3\text{N}_4/\text{MoS}_2$ nanocomposite exhibited the improved dispersibility and stability. Specially, a small amount of $g\text{-C}_3\text{N}_4/\text{MoS}_2$ could reduce the wear and friction of paraffin oil tremendously under a load of 10N.

The $g\text{-C}_3\text{N}_4/\text{MoS}_2$ nanocomposite inherits both the preeminent lubricating properties of MoS_2 and the outstanding wear-resistant performances of $g\text{-C}_3\text{N}_4$ nanosheets. Importantly, $g\text{-C}_3\text{N}_4/\text{MoS}_2$ can easily move into the interface of the friction pair with oil and form a lubricating film during the sliding, preventing the direct contact between asperities. Therefore, the combination of MoS_2 with $g\text{-C}_3\text{N}_4$ is an effective way to improve the tribological properties, which has a promising prospect in the lubricant additive.

References

- [1] D. Berman, A. Erdemir, A. V. Sumant, *Mater Today*. **31**, 17 (2014).
- [2] J. Wei, M. Cai, F. Zhou, W. Liu, *Tribol Lett*. **521**, 53 (2014).
- [3] T. W. Scharf, S. V. Prasad, *J Mater Sci*. **511**, 48 (2013).
- [4] V. Eswaraiyah, V. Sankaranarayanan, S. Ramaprabhu, *ACS Appl. Mater. Interfaces.*, **4221**, 3 (2011).
- [5] J. Yang, Y. Xia, H. Song, B. Chen, Z. Zhang, *Tribol Int*. **118**, 105 (2017).
- [6] K.-S. Kim, H.-J. Lee, C. Lee, S.-K. Lee, H. Jang, J.-H. Ahn, J.-H. Kim, H.-J. Lee, *ACS Nano*. **5107**, 5 (2011).
- [7] J. Zhu, P. Xiao, H. Li, S. A. C. Carabineiro, *ACS Appl. Mater. Interfaces*. **16449**, 6 (2014).
- [8] L. Zhu, Y. Wang, F. Hu, H.J. Song, *Appl Surf Sci*. **349**, 345 (2015).
- [9] J. Yang, H.T. Zhang, B.B. Chen, H. Tang, C. S. Li, Z. Z. Zhang, *RSC Adv*. **64254**, 5 (2015).
- [10] G. Colas, A. Saulot, C. Godeau, Y. Michel, Y. Berthier, *Wear*. **192**, 305 (2013).
- [11] K.H. Hu a,b, J. Wang c, S. Schraube, Y. F. Xu, X.G. Hu, R. Stenglard, *Wear*. **1198**, 266 (2009).
- [12] J. Chen, Y. Xia, J. Yang, *Mater. Lett*. **248**, 210 (2018).

- [13] H. Li, J. Wang, S. Gao, Q. Chen, L. Peng, K. Liu, X. Wei, *Adv. Mater.* **1701474**, (2017).
- [14] K.M. Hou, J.Q. Wang, Z.G. Yang, L. Ma, Z. Wang, S. Yang, *Carbon*. **83**, 115 (2017).
- [15] I. Leven, D. Krepel, O. Shemesh, O. Hod, *J. Phys. Chem. Lett.* **115**, 4 (2013).
- [16] J. Q. Qin, C. W. Yang, M. Cao, X. Zhang, S. Rajendran, S. Limpanart, M. Ma, R. Liu, *Mater. Lett.* **156**, 189 (2017).
- [17] K.L. Gong, X.H. Wu, G.Q. Zhao, X. B. Wang, *Tribol Int.* **1**, 110 (2017).
- [18] Z.Y. Chen, H.X. Yan, T.Y. Liu, S. Niu, *Compos Sci Technol.* **47**, 125 (2016).
- [19] L. Guan, F.X. Tan, B.K. Lv, M. Wu, R. Wang, Y. Lu, X. Li, Z. Li, F. Teng, *Opt Commun.* **35**, 7 (2017).
- [20] T. Giannakopoulou, I. Papailias, N. Todorova, N. Boukos, Y. Liu, J. Yu, C. Trapalis, *Chem. Eng. J.* **571**, 310 (2017).
- [21] Y. H. Fu, W. Liang, J. Q. Guo, H. Tang, S. Liu, *Appl Surf Sci.* **9**, (2017).
- [22] J. Li, E. Z. Liu, Y. N. Ma, X. Hu, J. Wan, L. Sun, J. Fan, *Appl Surf Sci.* **694**, 364 (2016).
- [23] G. Y. Bai, J. Q. Wang, Z. G. Yang, H. Wang, Z. Wang, S. Yang, *RSC Adv.* **4**, (2014).